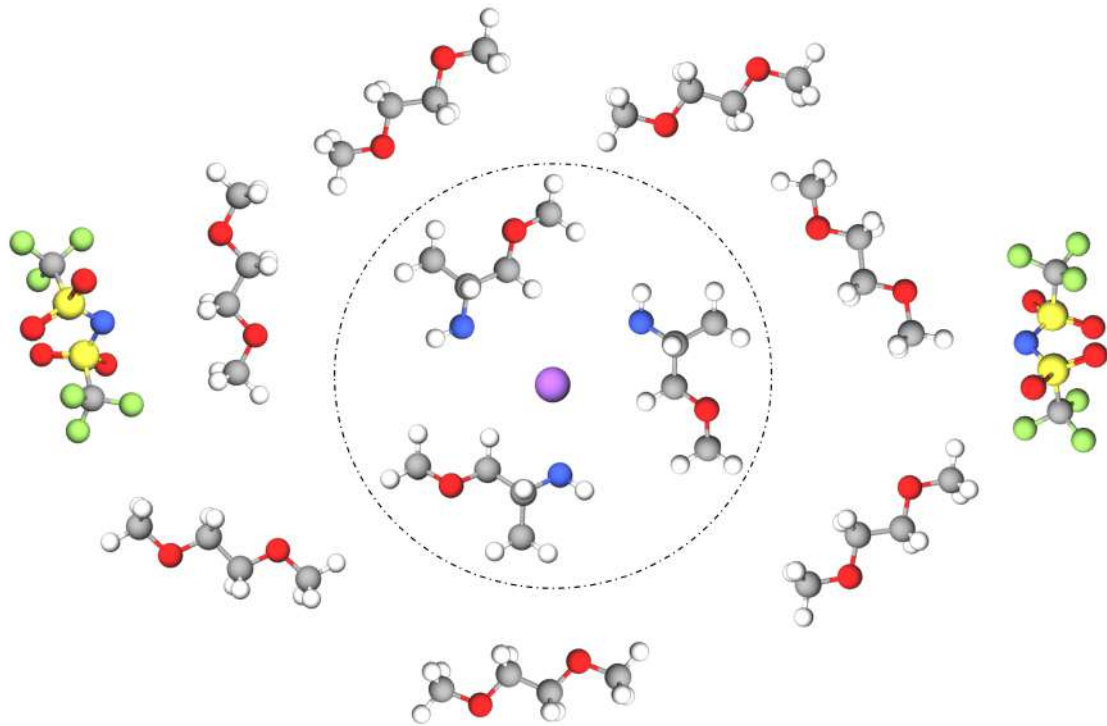




CHALMERS
UNIVERSITY OF TECHNOLOGY



Electrolyte design for rechargeable magnesium batteries

Methoxyethyl-amine chelants as electrolyte additives

Master's thesis in physics

LOVA WILSKE

DEPARTMENT OF PHYSICS

CHALMERS UNIVERSITY OF TECHNOLOGY
Gothenburg, Sweden 2022
www.chalmers.se

Electrolyte design for rechargeable magnesium batteries
Methoxyethyl-amine chelants as electrolyte additives
LOVA WILSKE

© LOVA WILSKE, 2022.

Supervisor: Jan Bitenc, National Institute of Chemistry, Ljubljana
Examiner: Patrik Johansson, Chalmers University of Technology, Department of
Physics

Master's Thesis 2022
Department of Physics
Division of Materials Physics
Chalmers University of Technology
SE-412 96 Gothenburg
Telephone +46 31 772 1000

Cover: Solvation structure of an RMB electrolyte, showing a Mg^{2+} ion in its first solvation shell provided by three 1-methoxy-2-propylamine molecules. The figure is a schematic representation and not based upon experimental or computational data. Elements are represented by the following colours: grey - C, green - F, white - H, pink - Mg, blue - N, red - O and yellow - S.

Abstract

Rechargeable magnesium batteries (RMBs) have been pointed out as promising candidates for future electrical energy storage and conversion system due to high theoretical volumetric energy density, low tendency of Mg metal anode to form dendrites, and the high abundance of Mg in the Earth's crust. Today's RMBs, however, suffer from low coulombic efficiencies and poor cycle life. Finding suitable electrolytes is the key to overcome these issues. A recently discovered family of electrolyte additives, methoxyethyl-amine chelants, has shown to improve battery performance by providing Mg^{2+} ion selective first solvation shells. This thesis aims to further explore the properties of these additives by evaluating their compatibility and performance with other electrolyte components and electrode materials, study the imposed morphology of deposits, and conduct EIS analysis to gain insight to the transport properties.

Galvanostatic cycling experiments show that 2-methoxyethyl-amine (M3) and 1-methoxy-2-propylamine (M4) increase the coulombic efficiency and lowers overpotential for 0.5 M $\text{Mg}(\text{TFSI})_2$:glyme systems. Mean Coulombic efficiencies up to 97% for first 100 cycles were recorded for $\text{Mg}||\text{SS}$ cells. The additive also displays good performance with the organic cathode material PAQS-CNT. Best performance is achieved with electrolytes with a 1:6 molar ratio between the Mg^{2+} ions and the additive. Surprisingly, these electrolytes separate into two immiscible phases.

Mg metal deposits formed in the presence of the additive are generally larger and exhibit higher Mg purity as shown by SEM and EDS analysis. This indicates that the additive suppresses side reactions and imposes good ion transport at the electrode surface. The very same conclusion was drawn from the EIS analysis, where the interfacial impedance was found to be remarkably low for electrolytes containing the additive.

Acknowledgements

First, I would like to direct my thanks to Robert Dominko and Patrik Johansson for giving me the opportunity to travel to beautiful Ljubljana for this interesting project and for sharing your knowledge. Next, my thanks goes to the battery group here at NIC. Thank you for all guidance in the lab and the good spirit. Last but not least, thanks to my supervisor Jan Bitenc - I have been so happy to have you to guide me through the landscape of magnesium batteries and thanks for all your good answers to my many questions.

Lova Wilske, Ljubljana, June 2022

Table of Contents

1	Introduction	2
1.1	Aim	3
2	Theory	4
2.1	Working principle of an electrochemical cell	4
2.1.1	Electrolyte	6
2.1.2	Performance measures	7
2.2	Characterization methods	8
2.2.1	Galvanostatic cycling	8
2.2.2	Microscopy and elemental mapping	8
2.2.3	Electrochemical impedance spectroscopy	9
2.3	Rechargeable magnesium batteries	10
2.3.1	Methoxyethyl-amine chelants as electrolyte additives	12
3	Methods	14
3.1	Chemicals and materials	14
3.2	Experimental setups and sample preparation	17
4	Results and Discussion	20
4.1	Cycling performance of RMBs	20
4.1.1	Electrolyte variations	21
4.1.2	Current density	26
4.1.3	Organic cathode	27
4.2	Morphology and composition of Mg deposits	28
4.3	Electrochemical detailed analysis	31
5	Conclusions and Outlook	34

1

Introduction

The ongoing climate crisis commands for development and implementation of sustainable energy solutions. High performant batteries based on abundant resources are needed for electrical energy storage and conversion systems [1]. The lithium-ion battery (LIB) is currently the rock star on the scene of commercially available battery technologies owing, to its high energy density and long lifetime. The materials which LIBs are based upon, however, raise concerns. The Li mining process is highly energy- and water-demanding, while Co, widely used in LIB cathodes, is a rare metal and the use of it has been frequently questioned due to unethical conditions for mine workers [2]. Apart from this, LIBs are also hampered by safety issues. It is therefore warranted to explore the potential of chemistries beyond LIBs: Li-S, Li-air, Na, K, Zn and the multivalent [3]: Mg, Ca and Al.[1] [4]

Rechargeable magnesium batteries (RMBs) have emerged as a promising candidate for next generation batteries due to the high theoretical volumetric capacity of the Mg metal anode (3832 mAh/cm³, vs Li at 2062 mAh/cm³), stemming from the divalent nature of the Mg ion. Furthermore, Mg is the 8th most common element in the Earth's crust and 300 times more abundant than Li and is therefore sustainable and cheap to apply in batteries. The RMB chemistry is also regarded as safer than that of LIBs due to Mg's low tendency to form dendrites [5]. All of this combined makes RMBs a competitive alternative to LIBs, but there are quite some challenges to overcome before this can become a reality. Today's RMBs suffer from low Coulombic efficiencies and poor cycle life. The complications originate in the Mg ions inability to migrate through solid surface films, while the anode surface at the same time is extremely reactive. [6] This provides a great challenge when it comes to electrolyte design. A recently discovered family of electrolyte additives, methoxyethyl-amine chelants, has shown to improve RMB performance [7]. The researchers behind the discovery propose that the beneficial effects originate in an ability of the additive to form Mg²⁺ selective solvation shells for ion transport. These additives and their possible effects on ion transport poses an interesting topic for further investigations.

1.1 Aim

This thesis aims to further explore the properties of methoxyethyl-amine chelants as additives for RMB electrolytes. This is made by three approaches:

1. Evaluation of the additives' compatibility and performance with various electrolyte components and electrode materials.
2. Study the imposed morphology and composition of deposits.
3. Conduct EIS analysis for different electrolytes to gain insight into the ion transport properties in the bulk electrolyte and at the electrode surface.

First a literature study is presented, followed by a description of the experimental procedures, the results and their interpretation, and finally the conclusions drawn. The hope is that the findings will deepen the understanding of the additives effects and thereby contribute to future electrolyte design for RMBs.

2

Theory

Alessandro Volta's demonstration of the voltaic pile in 1799 marks the birth of the battery. The following chapter will be dedicated to recount some of the findings from those who followed in Volta's footsteps. The theory behind electrochemical cells - the basis of any battery, RMBs and some measurement techniques, will all be described in order to present the necessary background for the understanding of the thesis.

2.1 Working principle of an electrochemical cell

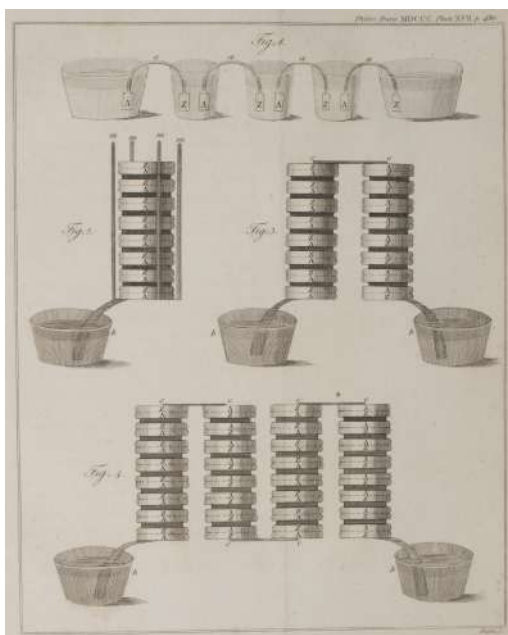


Figure 2.1: The drawing originates from a letter from Alessandro Volta sent to Sir Joseph Banks describing his invention. [8]

By exploiting the difference in *redox potential* between two pieces of metal Volta managed to produce a current of electrons to flow from Zn, by letting it undergo *oxidation*, to Cu which in turn switched to a *reduced* state. The metal pieces were in contact with a salt solution through which ions could flow. During discharge, cations reacted upon the Cu surface, neutralising the charge and provided a driving force for the process to continue. The steps of oxidation, reduction and the redox

reaction itself is presented in following equations:

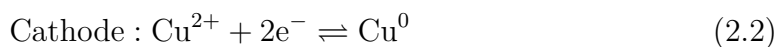


Figure 2.1 displays Volta's drawing of his invention. Battery science has in the 200 following years evolved onto technologies more refined than the Voltaic pile, but the working principle upon which the cells are based remains the same.

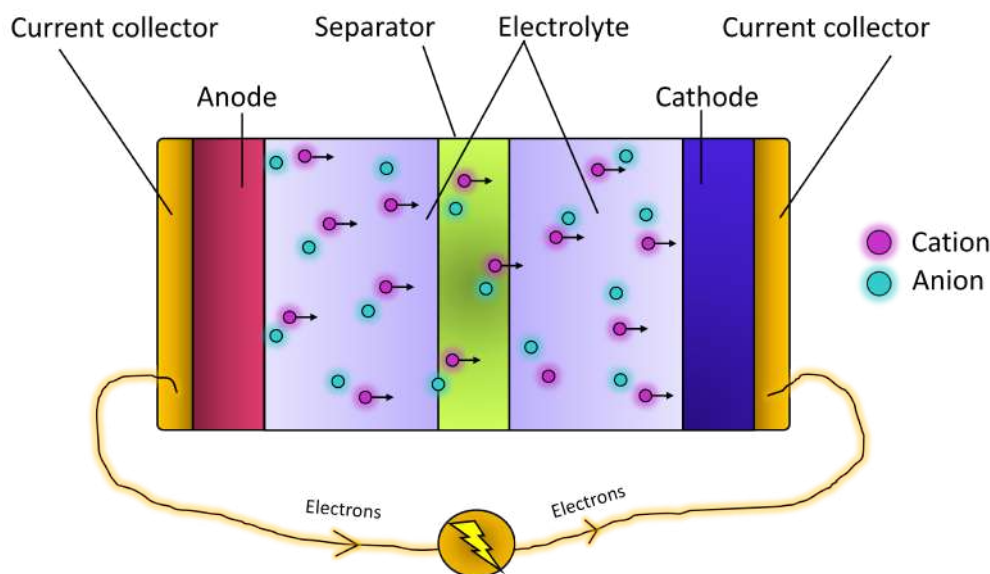


Figure 2.2: Schematic figure of a discharging electrochemical cell consisting of electrodes, electrolyte, separator and current collectors. Electrons flow through an external circuit while ions flow through the electrolyte.

A battery consists of several electrochemical cells. Connecting electrochemical cells in series increases the battery voltage while connecting them in parallel will realise a higher current and thus higher power performance. This study concerns electrochemical cells built up by following configuration: two electrodes with electrolyte and separators placed between them and current collectors enabling electric current to flow through an external circuit as presented in Figure 2.2. The electrode undergoing oxidation during discharge of the cell is referred to as *anode* and the one undergoing reduction is the *cathode*. The electrolyte conducts ions and blocks electrons from flowing through.

2.1.1 Electrolyte

A functional electrolyte is comprised of solvent, salt and additives. The solvents role is to dissolve the salt into cations and anions, while the additive can serve many purposes, for example generate stability in the solution, aid in forming an ion conducting solid electrolyte interphase (SEI), increase electrolyte safety, or establish a favourable solvation structure for the ions. Good ionic conductivity, electronic insulation, thermal and chemical stability, together with ample ion transport ability and transport at the electrolyte/electrode interface are essential properties of an electrolyte. [9]

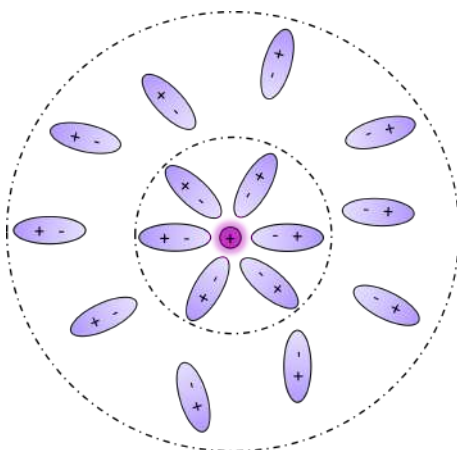


Figure 2.3: Solvation structure for a cation displaying its first and second solvation shell. The charge of ion and polarity of solvent are both arbitrary and not limited to the example displayed.

Ion transport is dependent on the solvation structure. The ions, pulled by the electrostatic force between the electrodes, will flow encapsulated by solvation shells (Figure 2.3). Their structure can vary, but the first solvation shell is generally the most ordered due to the field being stronger close to the ion. Solvents can be of different denticities, meaning that the number of electronegative sites vary. The denticity will affect the solvent's orientation and also how it arranges itself with respect to other solvating species. The cation-anion coordination also affects the solvation structure. Ions can either form contact ion pairs (CIPs) where both ions are in the first solvation shell, or solvent separated ion pairs (SSIPs) in which the ions are solvated solely by solvents. The distribution of CIPs and SSIPs is often concentration dependent, favouring CIPs at higher concentrations. [10] CIP coordination is more likely to result in anion decomposition at the anode surface than for the case of SSIPs. [11]

2.1.2 Performance measures

The total amount of electrical current extracted from an electrochemical cell is defined as its *capacity* and can be measured in units of Ah.

$$\text{Capacity} = \int_0^t I dt \quad (2.4)$$

where I is current and t time. Inclusion of weight gives the specific capacity and can be calculated accordingly:

$$Q = \frac{nF}{M_w} \quad (2.5)$$

n represent number of transferred electrons, which in case of Mg is 2. F is Faradays constant, 96485 C/mol, and M_w is molar weight, which is 24.3 g/mol for Mg. The theoretical specific capacity for the Mg anode is 2206 mAh/g.

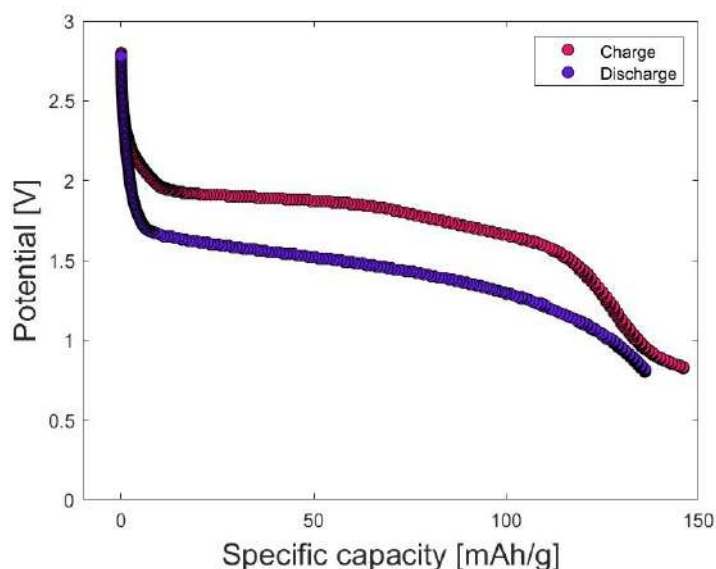


Figure 2.4: Schematic charge and discharge potential curves.

Reversibility of redox reactions is an important criterion for obtaining long cycle life for an electrochemical cell. Coulombic efficiency describes the reversibility for each cycle by comparing charge output with input.

$$\text{Coulombic efficiency} = \frac{\text{Discharge capacity}}{\text{Charge capacity}} \times 100 \quad (2.6)$$

The discharge capacity does not reach the charge capacity in Figure 2.4 which indicates a Coulombic efficiency below 100%. It can also be seen in the figure that potential for discharge is lower than during charge. This relates to the energy losses in the cell. Energy is calculated accordingly:

$$\text{Energy} = \int_0^t V(t) I dt \quad (2.7)$$

The loss of potential is referred to as *overpotential* and arises from inefficient mass and charge transport and reaction activation [12].

2.2 Characterization methods

The measurement techniques used to collect the data presented in Chapter 4 are here explained briefly.

2.2.1 Galvanostatic cycling

Galvanostatic cycling is a simple and useful technique for evaluating the performance of an electrochemical cell. Potential is recorded while the cell is being discharged and charged in cycles under a constant current. The experiment requires a working electrode (WE) and a counter electrode (CE). Discharge is initiated by applying a negative current to the WE. This will in Mg cells employing a stainless steel (SS) disk result in *plating* of Mg. The WE will then during discharge undergo *stripping* of Mg. Typical potential curves for plating and stripping of a Mg cell with a SS disk as WE is presented in Figure 2.5. Plating does not occur when cycling with an organic cathode as WE. The mechanism is instead based on *coordination* between Mg^{2+} and redox active sites in the organic host.

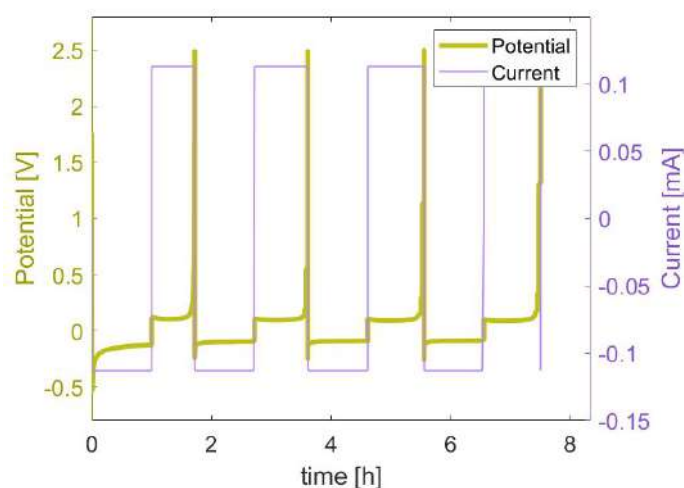


Figure 2.5: Four measured cycles in a typical galvanostatic cycling experiment.

2.2.2 Microscopy and elemental mapping

μm -nm scale topography images can be obtained by letting a beam of focused electrons raster scan a specimen and, by analysis of secondary electrons, reconstruct its surface. The technique is called scanning electron microscopy (SEM). Elemental specific morphology studies can be conducted when SEM is coupled with energy dispersion spectroscopy (EDS). If high enough powers are reached, the electron beam has the ability to kick out core electrons from the specimen atoms. Such an event will lead to a relaxation of electrons from outer shells, which in turn results in an X-ray photon being emitted. Since electron energy levels are quantized, the wavelength of the emitted photon will be unique for each element. By analysing the

emission spectra in terms of intensity at certain wavelengths, the material composition can be determined. Although, it should be noted that the elements that lack inner shells, H and He, can not be detected by an EDS instrument. EDS is considered a bulk measurement technique since the beam mainly ionizes electrons some μm below specimen surface. Beam penetration depth depends on the density of the specimen and applied beam energy. In order to conduct mapping of species closer to the surface, eg study surface films, other techniques such as X-ray photoelectron spectroscopy (XPS), provides a suitable complement.[13] Only SEM imaging and EDS measurements were conducted for this study.

2.2.3 Electrochemical impedance spectroscopy

Electrochemical impedance spectroscopy (EIS) is a technique that enables to study the frequency dependence of the impedance response of an electrochemical cell. The technique can in some cases even provide the experimentalist with insight on the impedance contribution of specific transportation steps. This in turn, can enable deduction of transport conditions for an electrolyte, the electrode surface as well as the transport and charge transfer inside the electrode. One way of performing an EIS measurement is to apply a small alternating potential over frequency spectra to a cell with identical electrodes. Such cells are called *symmetric cells*. EIS measurements can also be conducted by instead shifting the current, but this thesis will only include measurements of the first kind and the theory presented in this section will therefore focus on that. Nyquist plots provide a useful presentation for analysis of EIS data. The horizontal axis displays the real part of the impedance (resistance) and the vertical is the negative imaginary part of impedance (capacitance). An example of the frequency response of different components in a Nyquist plot is presented in Figure 2.6.

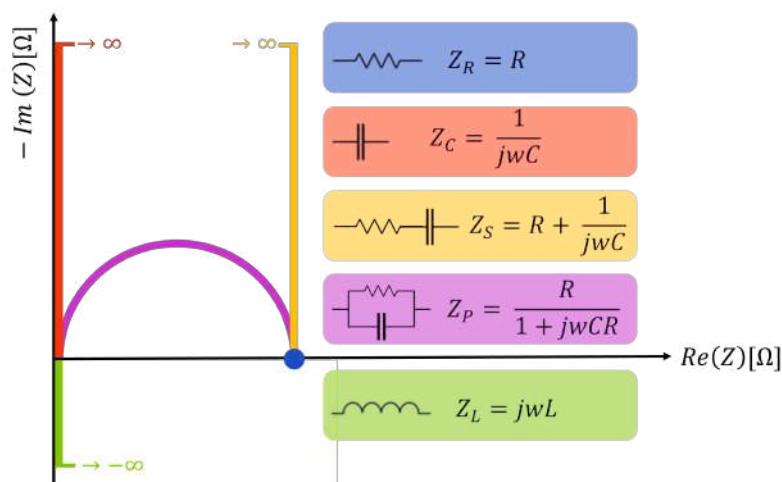


Figure 2.6: Nyquist response of different components.

Computational studies have shown that it is possible to model the impedance response of an electrochemical cell by finding an equivalent circuit of resistors and capacitors representing the different transport steps [14]. The configuration of

equivalent circuits depends on the electrode material, electrolyte and the chemical mechanisms within the cell. However, due to complexity, approximations must be made. No computational approaches will be attempted in this study, but the models provide an insightful tool for EIS data interpretation.

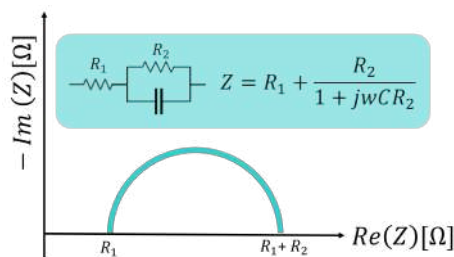


Figure 2.7: Nyquist response

Figure 2.7 shows an oversimplified model of a symmetric cell, where resistor R_1 represent the impedance provided by the electrolyte bulk and the resistor and capacitor connected in parallel represent the interfacial impedance. Interactions at the electrode surface are generally much more complex than in Figure 2.7, but the representation of electrolyte bulk resistance is accurate. Ionic conductivity, σ , of an electrolyte can be calculated accordingly:

$$\sigma = \frac{c}{R} \quad (2.8)$$

c is a constant specific for the cell dimensions in which the measurement was performed and the value R is the electrolyte bulk resistance which is given by the value where the arc intersects the horizontal axis. Interfacial impedance is the sum of contributions from multiple processes, such as electron conduction and ion interaction and reaction with the electrode and passive surface films [14]. The analysis of interfacial impedance included in this thesis will however only concern the sum.

2.3 Rechargeable magnesium batteries

The term 'rechargeable magnesium battery' (RMB) refers to rechargeable batteries that employ Mg^{2+} ions as the charge carrier of interest. The anode is for most RMBs based on Mg metal and this criterion will be adapted to the 'RMB' term throughout this thesis.

The first thing a scientist about to tackle RMB chemistry needs to know is that divalent ions, such as Mg^{2+} , suffer from the inconvenience of not being able to migrate through SEIs. [6] This means that any reaction between electrolyte and electrode that forms a solid film will block Mg ions and inactivate the electrochemical process. Ion transport in LIB cells differs significantly from RMBs in this aspect. LIBs generally owes its high reversibility to the protective and yet Li^+ conducting SEI. The Mg ions disability in combination with the high reactivity of Mg metal poses a difficult task of finding suitable electrolytes. Having broken these intimidating news, we can now turn to some of the favourable aspects of RMBs. The divalency

of Mg^{2+} ions enables high anodic capacity. Mg metal also exhibits a relatively low reduction potential (-2.38 V vs. SHE, only 0.71 V higher than for Li^+/Li^0) which enables high voltage electrochemical cells.

The RMB timeline stretches back to 1929, when ethereal Grignard solutions were proven to enable Mg deposition [15]. However, the electrolytes suffered from low ionic conductivity and poor oxidative stability and it was not until 60 years later when Gregory et al. [16] presented their new collection of inorganic materials that another breakthrough in RMB research was accomplished. Today's RMB electrolytes are still ether-based, since these solvents have a relatively low tendency to react with the anode. The most popular ethers are glymes and tetrahydrofuran; polar aprotic solvents and suitable for cation transport. This study will focus on the two smallest molecules belonging to the glyme family – dimethoxyethane (DME) and bis(2-methoxyethyl) ether (diglyme) as solvents.

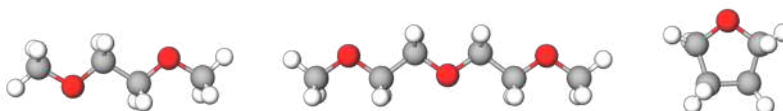


Figure 2.8: Ethernal solvents for RMB electrolytes: DME, diglyme and tetrahydrofuran (from left to right). Elements are represented by following colours: grey - C, white - H and red - O.

The discovery of the Chevrel phase as an Mg intercalative cathode material by Aurbach et al. in 2000 marks the next milestone [17] after Gregory's demonstration. Research efforts in cathode materials has since then split into three branches – inorganic, organic and sulfur compounds.[18] One of the organic materials that has received a great deal of attention is the polymer poly(anthraquinoyl sulfide) (PAQS) [19].

One of the most studied salts for RMB electrolyte applications is magnesium(II) bis(trifluoromethanesulfonyl)imide ($\text{Mg}(\text{TFSI})_2$). Electrolytes starring this salt in combination with ether solvents and MgCl_2 salt dominated the field for a period, reaching coulombic efficiencies up to 98% and overpotentials as low as 0.2 V [20]. Advantages of adding Cl salts such as MgCl_2 is that it stabilises Mg^{2+} ions, has the ability to some extent protect the Mg metal surface from the formation of passivating layers, and that it lowers the energy barrier during Mg plating and stripping, thus decreasing the overpotential of the cell [6]. There are however two major drawbacks associated with Cl – the first is problem with current collector corrosion [21] and the second is capacity loss. MgCl_2 would ideally dissolve into Mg^{2+} and 2Cl^- , but studies suggest that MgCl_2 -containing electrolytes will rather form MgCl^+ and $\text{Mg}_2\text{Cl}_2^{2+}$ [22], which thereby consumes the electrolyte of ions available for the redox process. Other efforts in finding suitable salts has focused on large complex salts with B-based anions. Zhao-Karger et al. presented in 2017 RMB cells of coulombic efficiencies above 98% with their electrolyte of $[\text{Mg}(\text{DME})_3][\text{B}(\text{hfip})_4]_2$ ($\text{Mg}(\text{Bhfip})_2$)[23]. hfip is short for hexafluoro-2- propanol. The bulky hfip anion exhibits a delocalized charge, which makes it coordinate very weakly to Mg^{2+} . This

increases salt solubility and further the electrolytes ionic conductivity [24].

A peculiar behaviour of the electrolyte separating into two immiscible phases has been observed for $\text{Mg}(\text{TFSI})_2$:DME. The phenomenon can be explained by a lowering of system energy through adjustments in DME conformer distributions for different salt concentrations. In the particular case of $\text{Mg}(\text{TFSI})_2$:DME systems it is energetically preferable to separate into a phase of a low salt concentration and a phase with high salt concentration and a specific DME conformer distribution. [25]

The many promises of dendrite-free deposition [26] of Mg have recently been questioned. [27] Dendrites are spear-like structures growing out from an electrode during plating and can in the worst case puncture the separator and cause a short circuit. It has been suggested that the lower tendency towards dendrite formation in RMBs stems from the low self-diffusion barriers associated with the Mg^{2+} ions.[5]

2.3.1 Methoxyethyl-amine chelants as electrolyte additives

Methoxyethyl-amine chelants were recently presented by Hou et al. as an excellent family of additives for RMB electrolytes [7]. The study explored many electrolytes and the most significant improvement in performance imposed by the additives was found for 0.5 M $\text{Mg}(\text{TFSI})_2$ dissolved in DME. Two of the methoxyethyl-amine chelant additives proves to increase performance the most were 2-methoxyethylamine, referred to as M3, and 1-methoxy-2-propylamine, referred to as M4, (Figure 2.9).



Figure 2.9: Methoxyethyl-amine chelant additives M3 (left) and M4 (right). Elements are represented by following colours: grey - C, white - H, blue -N and red - O.

Three of the electrolytes investigated by Hou et al. plays an important role in this thesis as well and they are the following:

- **E3:** 0.5 M $\text{Mg}(\text{TFSI})_2$ dissolved in DME and M3. The molar ratio between Mg^{2+} ions and M3 molecules is 1:4.
- **E4:** 0.5 M $\text{Mg}(\text{TFSI})_2$ dissolved in DME and M4. The molar ratio between Mg^{2+} ions and M4 molecules is 1:4.
- **E_{blank}:** 0.5 M $\text{Mg}(\text{TFSI})_2$ dissolved in DME. Baseline for comparison.

The abbreviations from the study of Hou et al. have been adopted to this thesis. The coulombic efficiency accomplished by $\text{Mg}||\text{SS}$ cells with electrolyte E4 was reported to reach an average of 99.5% spanning the 100 first cycles. Overpotentials as low as 0.1 V were reported. Hou et al. also studied the composition of surface species after cycling with XPS, and found that M3 and M4 effectively suppressed

decomposition of DME and to quite an extent also TFSI. The XPS result for E3 and E4 was in stark contrast with E_{blank} , where the amount of decomposed species were about 35 times higher.

Hou et al. attributed the improved performance to the additive's abilities to form Mg ion selective solvation shells. This claim was backed up by density functional theory (DFT) calculations of affinity of the solvating species, calculations based on Marcus theory predicting more polarisable solvation shells containing the additives, and experimental characterisation with nuclear magnetic resonance (NMR) and Raman spectroscopies.

3

Methods

To explore the effects of adding methoxyethyl-amine chelants in RMB electrolytes a variety of electrolytes containing different salts and solvents were prepared and studied in different experiments. Electrolytes containing the additives were also tested together with an organic cathode. All electrolytes were studied by galvanostatic cycling and the results constituted a foundation for which follow-up experiments were planned. Experimental procedures and the studied materials are presented in the following section.

3.1 Chemicals and materials

A summary of the used chemicals and where they were purchased is presented in table 3.1, followed by a list of all investigated electrolytes in table 3.2. Details of how materials were handled will also be presented in this section.

Drying DME

The procedure was performed inside a glovebox with a content of air and water below 0.1 ppm. All of the glassware used was dried at 200 °C. A commercial solvent (suitable for high-performance liquid chromatography, 99.9%, inhibitor-free) was dried with molecular sieves (4 Å). After that, 1 mL of Na/K alloy was added into 0.5 L of solvent and refluxed over the night. In the end, the solvent was fractionally distilled (125 °C, 1000 mbar). The remaining water content in the solvent was 1ppm.

Drying additives

M3 and M4 were dried with molecular sieves (4 Å) and stored inside the glove box. The procedure is copied from Hou et al. [7]

Synthesis of Mg(Bhfp)₂

The salt was synthesised by Tjaša Pavčnik in 2 steps. Mg(BH₄)₂ was synthesised according protocol by Zhao-Karger et al. [28]. The same protocol was followed in the second step as well, but with an additional modification: solvents and residual reactants were removed under vacuum after the reaction to obtain a concentrated solution. The concentrated solution was then slowly added into hexane, in which Mg(Bhfp)₂ salt precipitated. The salt was filtered and dried under vacuum for 24 h at 45 °C.

Synthesis of PAQS-CNT

The active material PAQS was synthesised by Olivera Lužanin according to the protocol by Song et al. [29]. Multi-walled carbon nanotubes (CNTs) were added and constituted 10 wt% of the final product. The purpose of CNT is to increase the electronic conductivity of the active material.

Table 3.1: Additives, solvents, salts and the active material used in the experiments. The last column states from where chemicals were obtained. Only structures of anions of the salts are presented. Colours of the atoms represent the following elements: grey - C, red - O, blue - N, yellow - S, light green - F, dark green - Cl, beige - B and white - H.

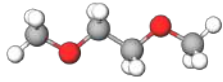
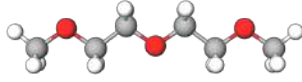
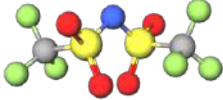
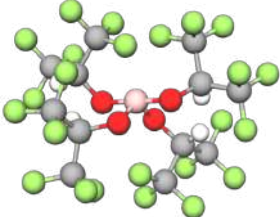
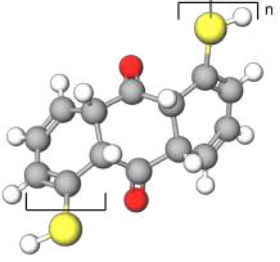
	Acronym	Chemical structure	Source, drying
Additives	M3		99%, Sigma-Aldrich
	M4		99%, Sigma-Aldrich
Solvents	DME		Sigma-Aldrich
	diglyme		Sigma-Aldrich
Salts	Mg(TFSI) ₂		Extra dry, Solvionic
	MgCl ₂		99.9%
	Mg(Bhfp) ₂		In-house synthesis
Active material	PAQS		In-house synthesis

Table 3.2: A complete list of all used electrolytes. The last column refers to molar relation between Mg ions and additive.

Acronym	Salt conc.	Salt	Solvent	Additive	Ratio
E3	0.5 M	Mg(TFSI) ₂	DME	M3	1:4
E4	0.5 M	Mg(TFSI) ₂	DME	M4	1:4
E _{blank}	0.5 M	Mg(TFSI) ₂	DME	-	-
	1, 0.5 M	MgCl ₂ , Mg(TFSI) ₂	DME	M3	~1:1.3
	1, 0.5 M	MgCl ₂ , Mg(TFSI) ₂	DME	M4	~1:1.3
	1, 0.5 M	MgCl ₂ , Mg(TFSI) ₂	DME	-	-
	0.32, 0.17 M	MgCl ₂ , Mg(TFSI) ₂	DME	M3	~1:4
	0.32, 0.17 M	MgCl ₂ , Mg(TFSI) ₂	DME	M4	~1:4
	0.32, 0.17 M	MgCl ₂ , Mg(TFSI) ₂	DME	-	-
	0.2 M	Mg(Bhfp) ₂	DME	M3	~1:10
	0.2 M	Mg(Bhfp) ₂	DME	M4	~1:10
	0.2 M	Mg(Bhfp) ₂	DME	-	-
	0.5 M	Mg(TFSI) ₂	Diglyme	M3	1:4
	0.5 M	Mg(TFSI) ₂	Diglyme	M4	1:4
	0.5 M	Mg(TFSI) ₂	Diglyme	-	-
E _{4lowM4conc.}	0.5 M	Mg(TFSI) ₂	DME	M4	1:1
E _{4mediumM4conc.}	0.5 M	Mg(TFSI) ₂	DME	M4	1:2
E _{4highM4conc.}	0.5 M	Mg(TFSI) ₂	DME	M4	1:6
E _{4doubleM4conc.}	0.5 M	Mg(TFSI) ₂	DME	M4	1:8
	0.5 M	Mg(TFSI) ₂	Diglyme	M4	1:1
	0.5 M	Mg(TFSI) ₂	Diglyme	M4	1:2
	0.5 M	Mg(TFSI) ₂	Diglyme	M4	1:6
	1 M	Mg(TFSI) ₂	DME	M4	1:4

3.2 Experimental setups and sample preparation

Electrolytes were studied through galvanostatic cycling using *Swagelok cells* (Figure 3.1).

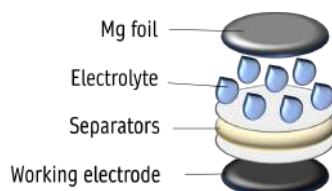


Figure 3.1: Cell structure features working electrode, 3 separators, electrolyte and Mg metal foil.

Electrolyte preparation

All electrolytes and cells were prepared inside a dry glovebox (1-5 ppm H_2O) filled with Ar to keep an inert environment. Vials were dried for more than 12 h in an oven at 80 °C before they were entered to the glovebox. Salt was added to a volumetric flask and liquid of solvent and additive was poured on top.

Cell assembly

The working electrode (SS disk in most cases) was placed in the bottom of the Swagelok cell with separators on top. Celgard separators were in contact with electrodes for both sides and a glassy fibre Whatman GF/A separator was placed in between. Electrolyte was added by glass pipette, 7 drops for most cells. Mg foil was brushed before placed in the cell in order to clear the surface from oxides. The cell was then closed and tightened with wrenches.

Cathode preparation

PAQS-CNT is mixed with printex and a polytetrafluoroethylene (PTFE) binder in weight proportions: 60% PAQS-CNT, 30% printex and 10% PTFE. Isopropanol was added to the mixture which was then ball-milled for 30 min at 300 rpm. The obtained slurry was placed on a board and cut into thin electrodes. The electrodes were thereafter dried in an oven at 50 °C before being transferred into the glovebox.

Galvanostatic cycling

Experiments were performed on VMP3 and MPG2 potentiostats from Bio-Logic S and data was processed with associated software. SS discs and cathodes of PAQS-CNT were employed as working electrodes in different experiments. SS disks are easy to work with and have the benefit of being compatible with all electrolyte and were therefor used as the standard experiment to compare the electrolytes.

The properties of most interest were the Coulombic efficiency, overpotential. Cycle life can also be of interest, but since consistent results can not be reached it is not suitable to conduct quantitative comparisons. The cycle life generally depend on local variations such as irregularities at the electrode surface or impurities within the battery. Coulombic efficiency and overpotential measurements are more reliable

and provide a good foundation for comparison. Graphs with selected measurements were prepared in Matlab.

SEM and EDS: preparation and analysis

A carbon coated aluminium foil was used in order to get deposits to stick. A Swagelok cell was prepared and Mg depositing was conducted for 2 h at a current density of 0.1 mA/cm^2 . The cell was then opened inside the glovebox where the electrode was washed with DME and left to dry before pieces of it was mounted upon the specimen holder, see Figure 3.2. The specimens were then transferred under vacuum to the chamber of the SEM and EDS instruments.

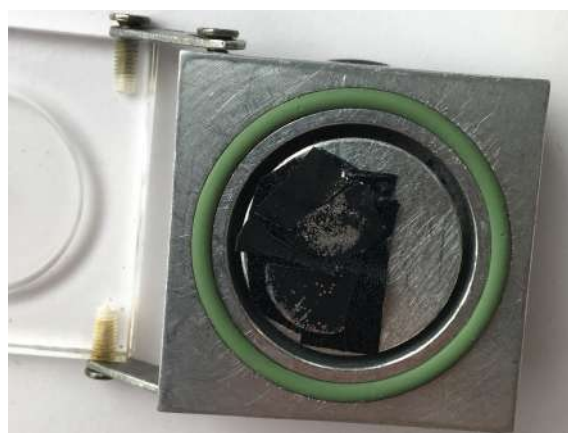


Figure 3.2: Specimen holder for SEM/EDS study with cycled electrodes placed upon carbon tape. The silvery deposits obtains high a Mg content.

The sample holder was not opened until vacuum had established in order to prevent air contamination. The morphology study was initiated with SEM imaging, instrument of type Supra VP 35, Carl Zeiss, to get an overview of the general topography before specific sites was targeted. Imaging was followed by EDS analysis of selected areas. 10 kV acceleration potential was applied which results in a $20 \mu\text{m}$ penetration depth. Analysis of spectra was conducted automatically with software provided by Oxford instruments, although, small manual modifications was added.

EIS

EIS measurements were performed with both Swagelok cell and in a costume designed cell for conductivity measurements. For the prior, symmetric cells with brushed Mg foil was employed. The rest of the cell configuration was identical to Figure 3.1. It is common knowledge that the measurement will be affected by the amount of time passed between assembly and measurement. This is caused by interactions between electrolyte and electrode. To minimise this influencing the results, experiments were all started approximately 10 min after assembly was completed. It should be noted that measurements had consistency issues even though this precaution was made. Specific values differed, but trends between different electrolyte remained. Ionic conductivity was obtained by measuring electrolyte bulk resistance



Figure 3.3: Conductivity cell assembled and disassembled. Electrolyte is only in contact with walls of plastic mid-section, cap and current collectors.

with the cell shown in Figure 3.3 and insert in eq 2.8. Cell constant c was obtained by measuring a reference solution with a known ionic conductivity (0.1 M KCl in water).

4

Results and Discussion

This study aims to shed light on the properties of RMB electrolytes containing additive M3 and M4. The project started off with an attempt of replicating galvanostatic cycling results reported by Hou et al. [7] Same materials, concentrations and preparation procedures were employed but our results did not entirely match theirs. The project thereafter went into an exploration phase. The properties of interest can be divided into three categories; 1) changing cell composition and electrolyte parameters and comparing performance in galvanostatic cycling, 2) exploring the morphology and composition of RMB cells after the first discharge and 3) study of impedance and ionic conductivity of the electrolytes.

4.1 Cycling performance of RMBs

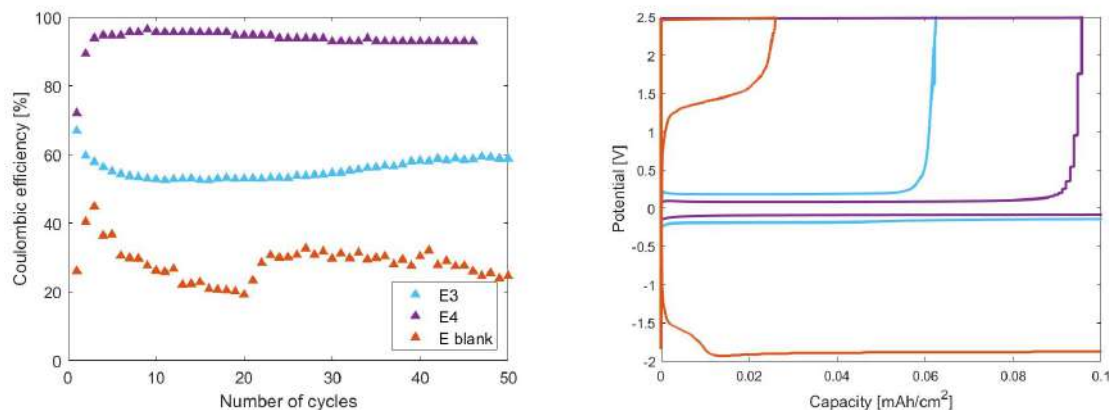


Figure 4.1: Galvanostatic cycling of Mg||SS cells with E3, E4 and E_{blank} electrolytes. The left graph shows the evolution of CE and the right displays the potential profile of the 10th cycle. A current of 0.1 mA/cm² was applied and the WE plating time was limited to 1 h. The cell with E3 has an average CE of 55.6%, E4 has 93.6% and E_{blank} has 28.3%.

The initial experiment of this study demonstrates that methoxyethyl-amine chelants have the ability to improve cycling performance for RMBs. The results, presented in Figure 4.1, show an increase in coulombic efficiency from 28.3% for E_{blank} to 93.6% for E4. A smaller effect was also observed for E3, although significantly lower than what had been reported by Hou et al. The additive also showed to

lower the overpotential, which is an indication of improved ion transport. Figure 4.1 displays the potential profile of the 10th cycle, but the same effect was observed throughout the cycling of the cells. Overpotential at the working electrode during plating was measured to be as low as 0.08 V for the cell containing E4 and this value is in agreement with results reported by Hou et al. However, the near 100% coulombic efficiency recorded for E3 and E4 was not possible to replicate using the same electrolytes and materials.

4.1.1 Electrolyte variations

In order to study additive–Mg(TFSI)₂ interactions without the influence of DME, electrolytes with a second solvent, diglyme, were prepared. Diglyme is known to have better compatibility with Mg(TFSI)₂ than DME. The result, see Figure 4.2, follows the same trend of additives improvement on performance, except for the coulombic efficiency obtained with additive M3. The experiment shows that the beneficial effects of the additives are not dependent on DME interactions.

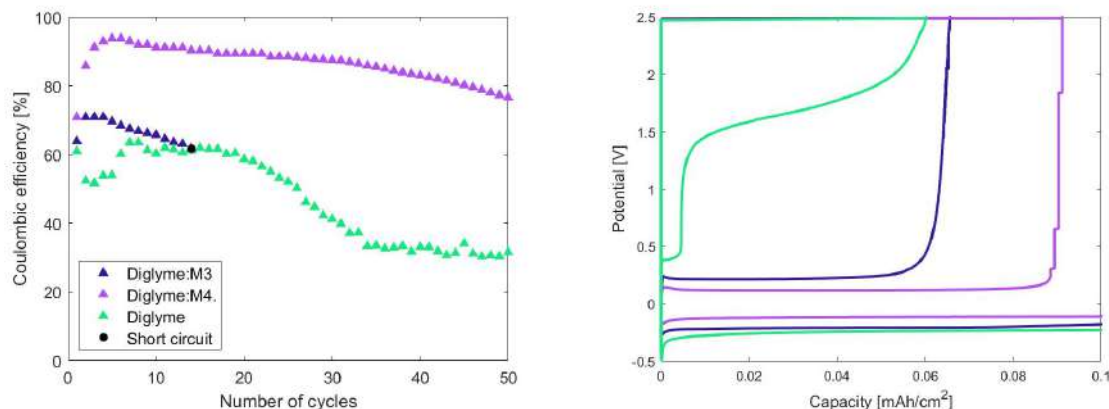


Figure 4.2: Galvanostatic cycling of Mg||SS cells with electrolytes of 0.5 M Mg(TFSI)₂ and solution mixtures of M3:diglyme, M4:diglyme and plain diglyme. Left graph shows the evolution of CE and the right displays the potential profile of the 10th cycle. A current of 0.1 mA/cm² was applied and WE plating time was limited to 1 h. The cell with M3 has a mean CE of 77.7%, M4 has 88.6% and plain diglyme has 47.0%.

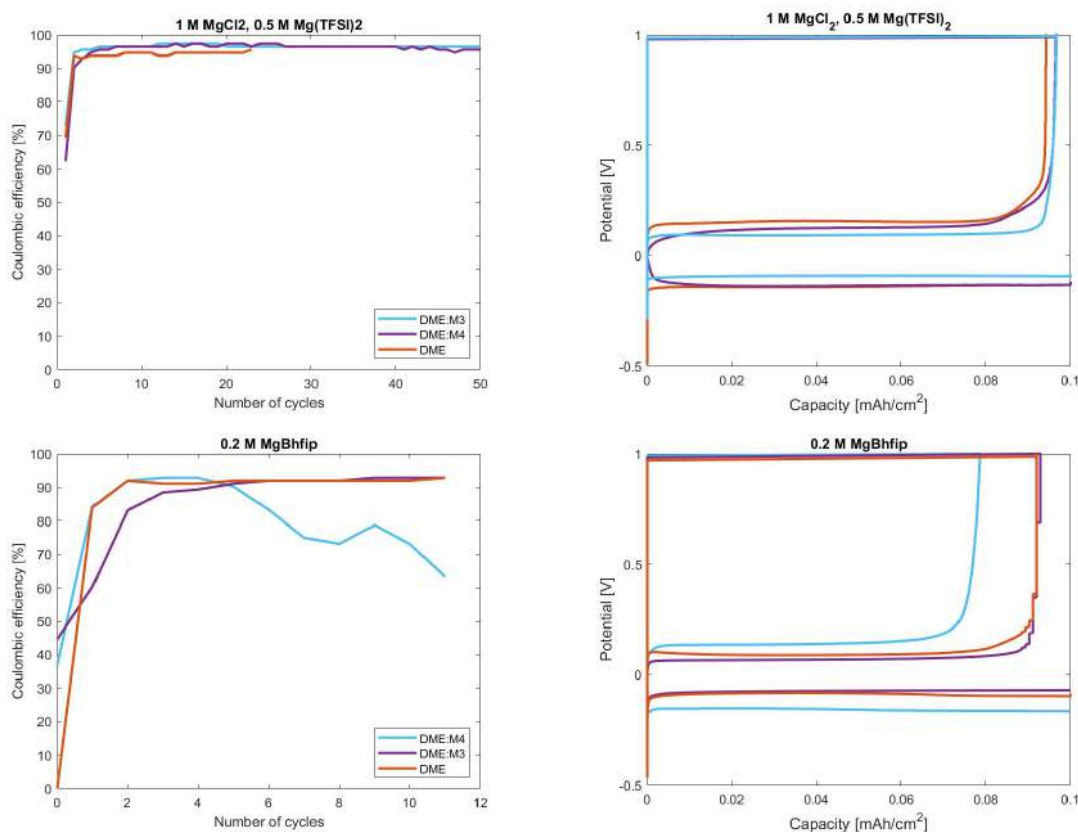


Figure 4.3: Galvanostatic cycling of Mg||SS cells with different electrolytes. The graphs form the basis for comparison of the effect of additives with different salts. Salt content is marked above the graphs and the legends display the solution mixtures. The left graph shows the evolution of CE and the right displays the potential profile of the 10th cycle. A current of 0.1 mA/cm² was applied and WE plating time was limited to 1 h. 1 M MgCl₂, 0.5 M Mg(TFSI)₂: Cell with M3 has a mean CE of 96.1%, M4 has 95.5% and plain DME has 93.3%. 0.2M Mg(Bhfp)₂: too few cycles to determine mean CE.

The next step towards gaining understanding of the behaviour of the methoxyethylamine chelants was to observe the additives compatibility with other salts. The selected salts, Mg(TFSI)₂-2MgCl₂ complexes and Mg(Bhfp)₂, are all well known for their good performance in RMBs. A comparison of the performance of the salts can be viewed in Figure 4.3. The additive decreases the performance for Mg(Bhfp)₂. One major difference between Mg(TFSI)₂ and Mg(Bhfp)₂ is the size of the salt – Mg(Bhfp)₂ is ~ 2.8 times heavier than Mg(TFSI)₂, leading to weaker coordination between ions. It would seem logical to reason that the Mg selectivity of the alleged solvation shell provided by the additive would increase for Mg(Bhfp)₂ due to its weak ion coordination and further enhance the protection of the electrode surface, but such effect was not observed. This raises an interesting question for future research of the role of additives in RMB electrolytes.

The performances of the electrolytes containing Mg(TFSI)₂-2MgCl₂ complexes are approximately the same for all three electrolytes, although slightly better for the electrolytes containing the additive. The ability to protect the Mg electrode surface

of Cl^- appears to play a more important role than the effect of the additive. In order to exclude high salt concentration from affecting the result, electrolytes containing 0.332 M MgCl_2 and 0.167 M $\text{Mg}(\text{TFSI})_2$ (Mg ion concentration adds up to 0.5 M) were run as well. The result displayed the same trend of performance as in Figure 4.3. The conclusion of the salt comparisons is that that electrolytes of 0.5 M $\text{Mg}(\text{TFSI})_2$ dissolved in glyme demonstrate the largest leap in performance by addition of methoxyethyl-amine chelants and variations of these systems were therefore selected for further studies. It is however possible that tuning the molar ratio between salt and additive could pave way for improved performance for $\text{Mg}(\text{Bhfp})_2$ and MgCl_2 -containing electrolytes, but such a study was not conducted during this thesis project.

E4 was chosen for further studies owing to its impressive increase in performance. The concentration of M4 in the electrolyte is one of the parameters that we suspect can influence its behaviour and we therefore prepared new variations of E4 and evaluated their performance in galvanostatic cycling. The M4 concentration in the initially investigated electrolyte has a 1:4 molar relation between Mg ions and additive. The following electrolytes were prepared and called accordingly

- **1:1** molar ratio between Mg ion and M4 - called E4 **low** M4 conc.
- **1:2** molar ratio between Mg ion and M4 - called E4 **medium** M4 conc.
- **1:4** molar ratio between Mg ion and M4 - called E4 **original** M4 conc.
- **1:6** molar ratio between Mg ion and M4 - called E4 **high** M4 conc.
- **1:8** molar ratio between Mg ion and M4 - called E4 **double** M4 conc.

The performances of various M4 concentrations can be deduced from Figure 4.4. E_{blank} is added to the figure for comparison.

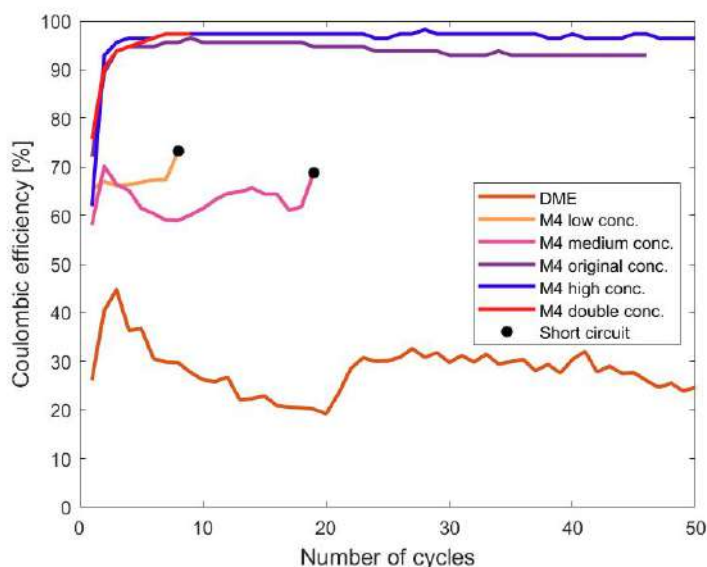


Figure 4.4: Galvanostatic cycling of $\text{Mg}||\text{SS}$ cells with conc. variations of E4 electrolytes. A current of $0.1 \text{ mA}/\text{cm}^2$ was applied and WE plating time was limited to 1 h. The cell with low M4 conc. has a mean CE of 67%, medium conc. has 63.1%, original conc. has 93.6%, high conc. has 96.3%, double conc. excluded.

The measurements of low and medium concentrations of M4 had to be run a few times to deduce the coulombic efficiency due to short circuiting during the first cycles. The short circuits were caused by dendrites that pierced through the separators, see Figure 4.6. A second batch of electrolyte with diglyme solvent was prepared and investigated as well and displayed a similar distribution of performances for added M4 concentrations, see Figure 4.5.

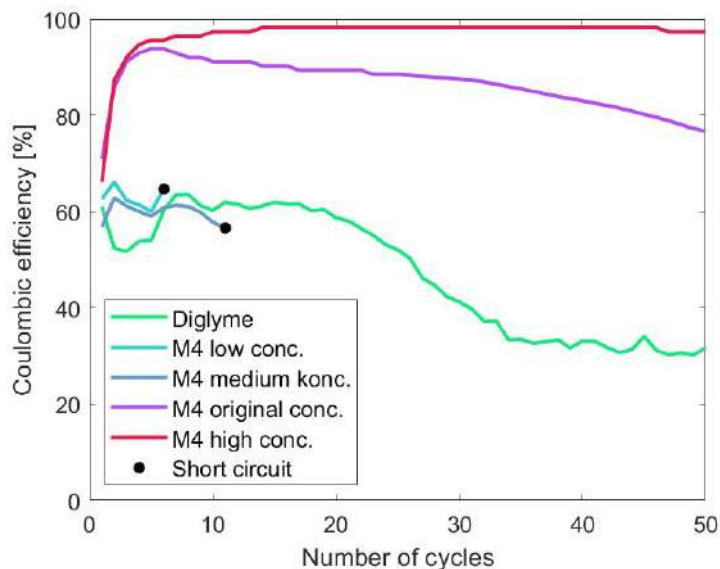


Figure 4.5: Galvanostatic cycling of Mg||SS cells with electrolytes of 0.5 M $\text{Mg}(\text{TFSI})_2$ and different solution mixtures of M4 and diglyme. A current of $0.1 \text{ mA}/\text{cm}^2$ was applied and WE plating time was limited to 1 h. The cell with low M4 conc. has a mean CE of 62.8%, medium conc. has 59.8%, original has 88.6% and high conc. has 96.8%

Short circuits during the first 11 cycles for cells containing electrolytes with low and medium M4 concentrations happened to 6 out of 8 cells. A possible explanation of the short cycle life could be that the amount of M4 is insufficient to protect the surfaces, but no unambiguous conclusion can be drawn since the cell failure also could originate from random disturbances.



Figure 4.6: Disassembled cell components (SS disk, 3 separators and Mg foil from left to right) of a short-circuited cell cycled with E4 medium M4 concentration. Dendrites have pierced the separators.

Another observation of interest from the M4 concentration variation experiments displayed in Figure 4.4 and 4.5 was the performance increase for cells containing a high M4 concentration. Coulombic efficiency for the electrolyte based on DME measured an average of 96.3% of the 50 first cycles and the electrolyte based on diglyme 96.8% (even 96.9% if the average instead is calculated for 100 cycles). Excess of M4 intuitively seems to be a good condition, but what introduces an element of confusion is that electrolytes with high M4 concentration exhibit phase separation, see Figure 4.7. The electrolyte was stirred before it was applied in the cell to ensure the application of the intended electrolyte composition. The state of the electrolyte once applied is unknown and raises an intriguing question. If the phase separation is still present, the electrolyte operates by a unique mechanism which I have not been able to locate in the literature.

The phase separated electrolytes were stored in volumetric flasks inside an Ar filled glovebox. After 30-40 days the phase separation disappeared. The event coincided with a nice and warm spring week and it might have been the temperature change that lead to the new miscibility of the phases. Phase separation has been previously reported for $\text{Mg}(\text{TFSI})_2$:DME electrolytes by Salama et al. [25], but not for systems with diglyme. Salama et al. concluded that the phase separation in their system was caused by a reorganisation of DME conformer distribution. Since the electrolytes of this project that exhibited phase separation were prepared with both DME and diglyme, the origin to the phase separation must be differently from what was reported by Salama et al. It is more likely that the phenomena arises from temperature differences. However, a closer study of the origin of the state change would have to be conducted to draw any conclusions and there was unfortunately no time.

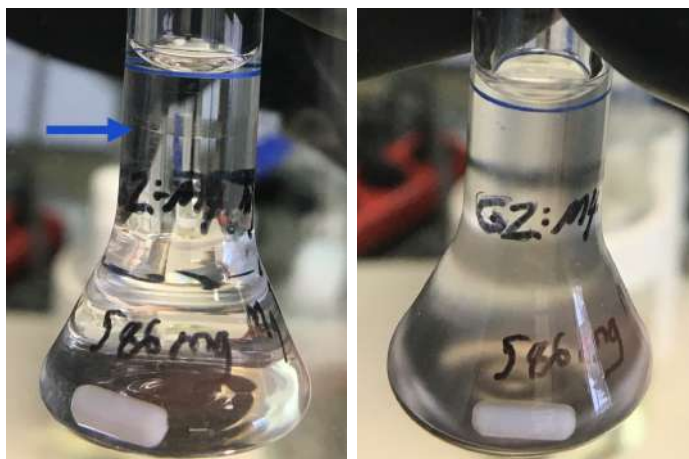


Figure 4.7: Freshly prepared electrolyte with high M4 conc. The left image shows the flask before it was stirred and the right one after stirring. A faint line between the phases can be seen in the left image.

It is worth mentioning that the electrolyte referred to as E4 double M4 conc. worked poorly. This confirms that peak performance was reached with the electrolyte referred to as E4 high M4 conc.

A quick investigation of the effect of salt concentration was conducted. An electrolyte of 1 M Mg(TFSI)₂ in DME:M4 with 1:4 relation between Mg ion:M4 (original M4 conc.) was prepared and applied in a Mg||SS cell. The shape of the potential curve of its 2nd discharge, see Figure 4.8, implies that the cell suffers from side reactions, which could be a consequence of poor Mg ion transport. The cell short circuited during its 11th cycle. One remarkable feature of the electrolyte with 1 M Mg(TFSI)₂ in DME:M4 is that it does not exhibit phase separation even though the volume ratio of added M4 is the same as in E4 double M4 conc., where phase separation is present. This indicates that the origin of the phase separation phenomenon is connected to the molar relation between additive and salt rather than additive to solvent. The molar ratio between Mg ions and M4 for which the phase separation first develops lies between 1:4 and 1:6.

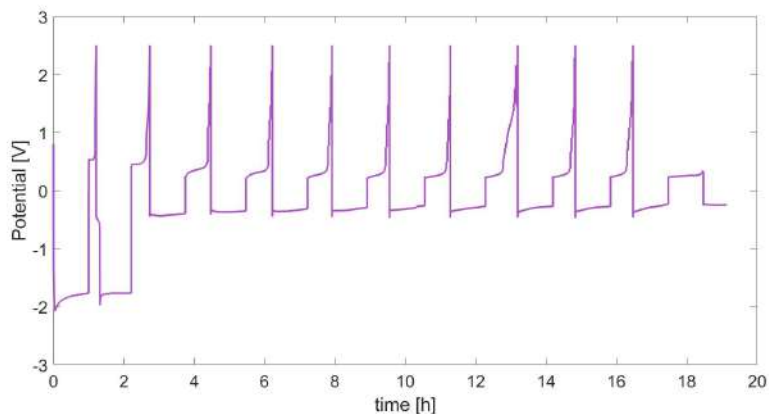


Figure 4.8: Galvanostatic cycling of a Mg||SS cell with 1 M Mg(TFSI)₂:DME electrolyte. The potential profile shows a sign of side reactions already during the 2nd discharge and the cell short circuits in its 11th cycle. A current of 0.1 mA/cm² was applied and WE plating time was limited to 1 h.

4.1.2 Current density

Galvanostatic cycling was mainly carried out at a current density of 0.1 mA/cm², which is considerably lower than commercial standards. Higher current densities were tested as well, with a dramatically shortened cycle life as a result. Dendrites were found to be the cause in several cells. A comparison of the nine first cycles run at 0.1 and 1 mA/cm² respectively is presented in Figure 4.9. The potential curves of the cells run at the higher current density display higher overpotentials and lower coulombic efficiencies. The features of these potential curves are also less defined which indicates the presence of side reactions which could be a consequence of insufficient ion transport. However, E3 sustained increasing current densities to a higher extent than E4 and even displayed coulombic efficiencies that exceeded experiments performed at 0.1 mA/cm². Experiments with other electrolyte variations were performed as well (diglyme, additive concentration variation) and they all showed poor resilience against higher current densities.

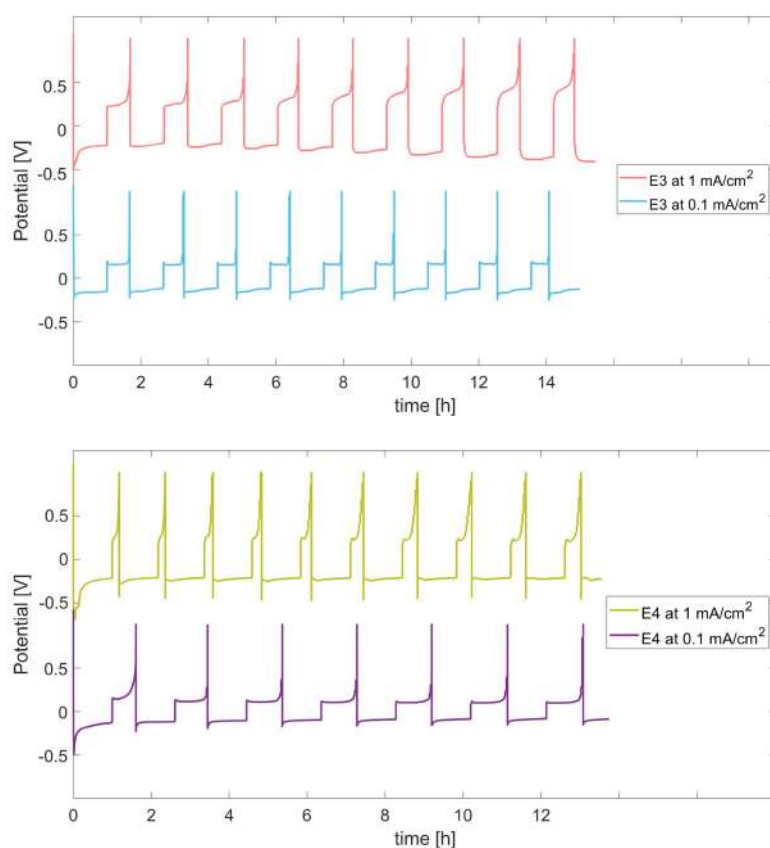


Figure 4.9: Potential curves for galvanostatic cycling of Mg||SS cells run at different current densities. Cells run at a higher current density have 2 extra glass fibre separators for protection against dendrites. Cycling was performed with an upper potential limit of 1 V. The plating overpotential for the cell containing E3 at 1 mA/cm² was measured to be 0.36 V and only 0.12 V at 0.1 mA/cm² and CE of the 5th cycle was 61.7% and 55.2% respectively. The plating overpotential for E4 at 1 mA/cm² was 0.22 V and only 0.08 V at 0.1 mA/cm² and CE of 5th cycle was 29.5% and 92.7% respectively.

4.1.3 Organic cathode

Compatibility between electrolyte and cathode material is essential in order for a cell to have practical meaning. To test this, cells with the organic cathode PAQS-CNT were assembled together with the different electrolytes, E3, E4 and E4_{highM4conc.}. Results from galvanostatic cycling of the cells are presented in Figure 4.10. The highest capacity was reached by the cell containing E3. E4_{highM4conc.} performed the best in regard to coulombic efficiency, which is in line with the previously presented experiment conducted with a SS disk. E_{blank} was prepared as well but it was not possible to charge and discharge at 0.5 mS/C like the other cell and was therefore excluded from the investigation.

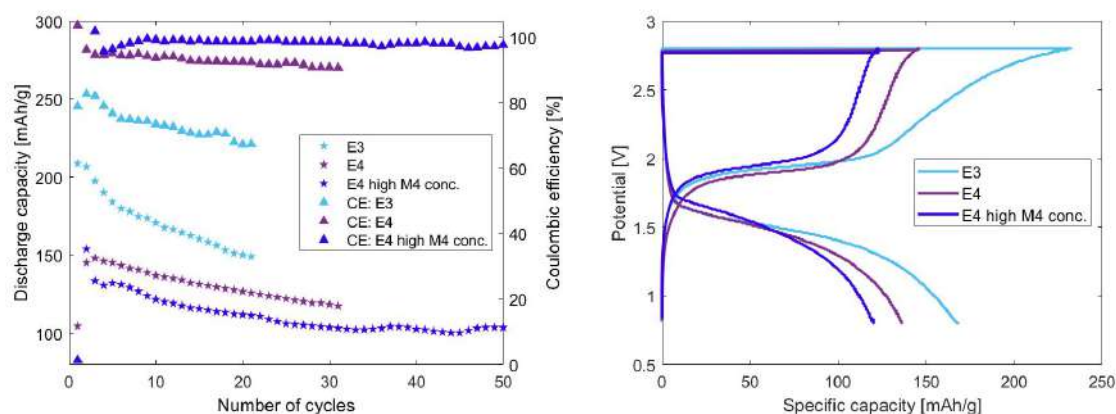


Figure 4.10: Galvanostatic measurements for cells with PAQS-CNT cathode and Mg anode. The three electrolytes employed are: E3, E4 and E4 with high M4 conc. The left graph shows how discharge capacity and coulombic efficiency varies during the measurement and the right graph shows the potential profile of the 10th cycle for all three cells. It should be noted that PAQS-CNT has a theoretical specific capacity of 225 mAh/g. Cells were run at 0.5 C.

4.2 Morphology and composition of Mg deposits

Mg was plated onto carbon-coated working electrodes and studied under SEM and EDS. The plated Mg formed deposits ranging from a μm to a mm scale. Deposits from cells containing electrolytes E3, E4 and E_{blank} were studied and their morphologies and compositions were compared. Figure 4.11 displays an overview of deposits from cells with the three electrolytes. Regions that represent the general appearance of deposits from each electrolyte were selected. The dark grey background is the carbon-coated electrode and the light grey regions are the deposits. The rough pattern on the deposits is an imprint of the separator structure.

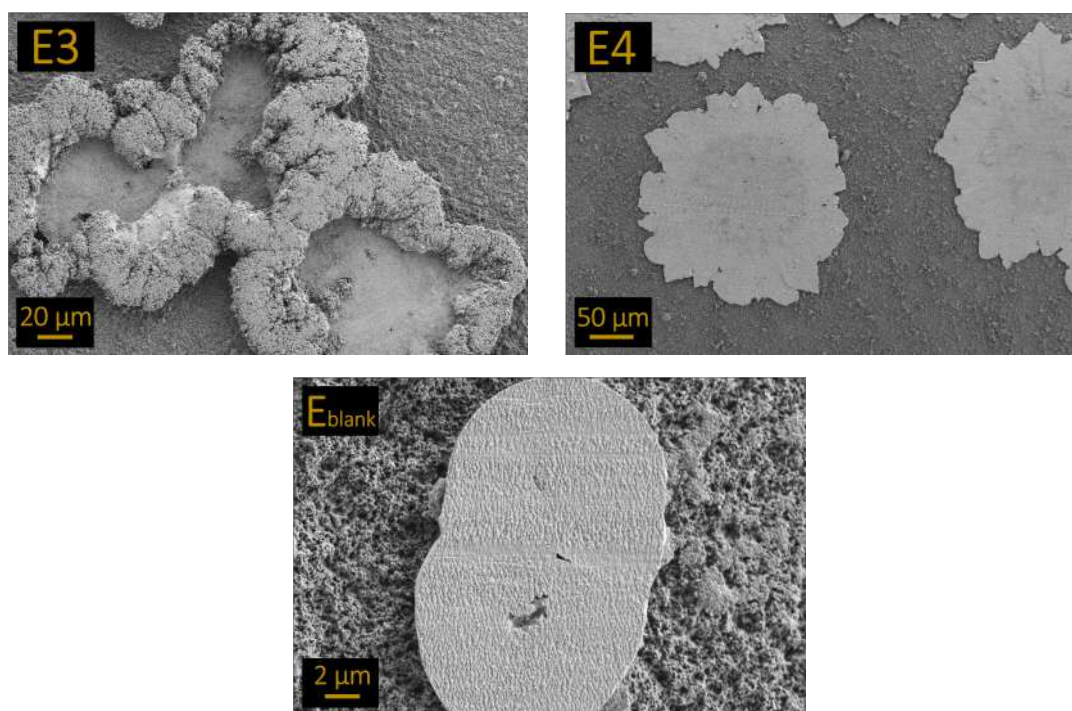


Figure 4.11: Overview of deposits from cells with E3, E4 and E_{blank} electrolyte at spots representing the general appearance from each cell. Note that the scale differs between images.

Deposits from E3 and E4 were generally larger than the ones from E_{blank} . It was also noted that the deposits formed in E3 cells obtained a different morphology. The deposits have edges of a porous structure in contrast to the main body, which is denser. Studying the edges on a closer scale, see the upper right corner in Figure 4.12, reveals a collection of what appears to be flakes. Compared with the image of the deposit edge from the cell with E4, the flakes of M3 are distinctly less organised. The same holds true for edges of deposits formed in E_{blank} . A number of deposits formed in E_{blank} appear to be immersed in the electrode, see lower left corner in Figure 4.12.

An investigation of deposit composition was conducted in order to gain insight to how efficient plating is and how good different electrolytes are at suppressing side reactions. Comparing Mg purity is the key to gain this insight. The results from EDS measurements of deposits formed in the three electrolytes are presented in Figure 4.13. E4 deposits exhibit the highest Mg content and E_{blank} the lowest. The conclusion is consistent with the superior performance of E4 observed for galvanostatic cycling (Figure 4.1).

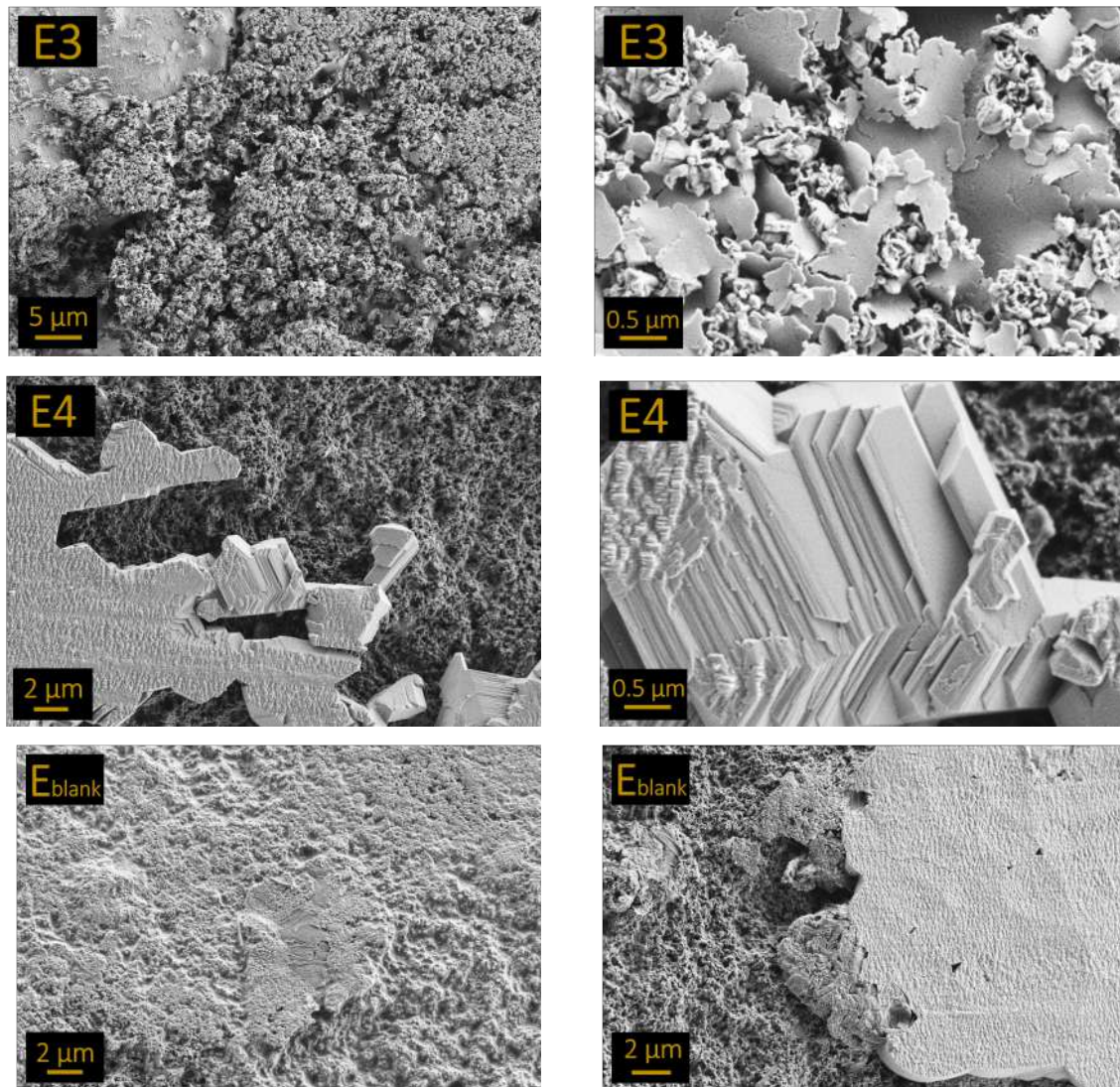


Figure 4.12: Deposits formed in cells with E3, E4 and E_{blank} electrolyte. Note that the scale differs between images.

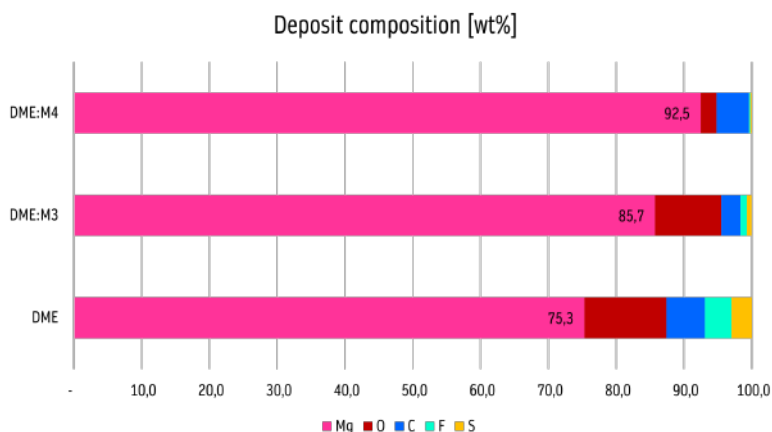


Figure 4.13: Composition of deposits formed in electrolytes E4, E3 and E_{blank} presented in wt%. Note that the instrument can not detect H.

No significant amounts of nitrogen were found, which would have been expected if either M3 or M4 would have decomposed on the electrode surface. This observation is interesting because it rules out the possibility of the additive serving a second purpose of creating an Mg-ion-conductive protective surface film. Although Hou et al. claim that the role of the additive is solely to enhance ion transport by providing an Mg ion selective solvation shell, the idea of a protective coating was still an interesting idea. The non-existing nitrogen content settles the idea to be highly unlikely.

If further morphology studies were to be performed, it would be advantageous to modify the experimental setup. The pressure of the separator on the electrode appears to have interfered with the formation of the deposits and aggravated the morphology interpretation. Swapping separators for spacers (inert plastic rings) might be preferable.

4.3 Electrochemical detailed analysis

The ability of M3 and M4 to increase coulombic efficiency, lower overpotential (Figure 4.1) and impose higher Mg purity for deposits (Figure 4.13) indicates that the additive improves transport of Mg ions. In an attempt to deduce how ion transport varies between the electrode surface and in the electrolyte bulk, EIS was performed on Mg symmetrical cells. The total resistance was found to be distinctly smaller for the electrolytes containing M3 and M4 than the ones without, see the Nyquist plot in Figure 4.14. More specifically, the diameter of arc features in the Nyquist plot, which relate to the interfacial impedance, decreases for the additive-containing electrolytes. The effect is largest for M4. The result is expected, since deposits formed in E4 were found to have a higher Mg purity. Decomposition of the electrolyte upon the electrode surface forms a passivating layer, which blocks ions from reaching the surface and thereby increases the interfacial impedance. If we instead turn our attention to the solution resistance of the Mg||Mg cells (high frequency

region displayed in the upper left corner of Figure 4.14), a rather surprising result appears. Electrolytes containing M4 exhibit significantly higher solution resistances, meaning that the ionic conductivity in the electrolyte bulk is lower. This indicates poor ion transport in the bulk and provides us with an insight that should be kept in mind while designing electrolytes for $\text{Mg}(\text{TFSI})_2$:glyme systems in RMBs — the interfacial ion transport has a greater impact on cycling performance than the ion transport in the bulk. Impedance measurements were also performed for 0.5 M $\text{Mg}(\text{TFSI})_2$:glyme electrolytes with different concentrations of M4 and a correlation between increasing M4 concentration and lowering of interfacial impedance was discovered.

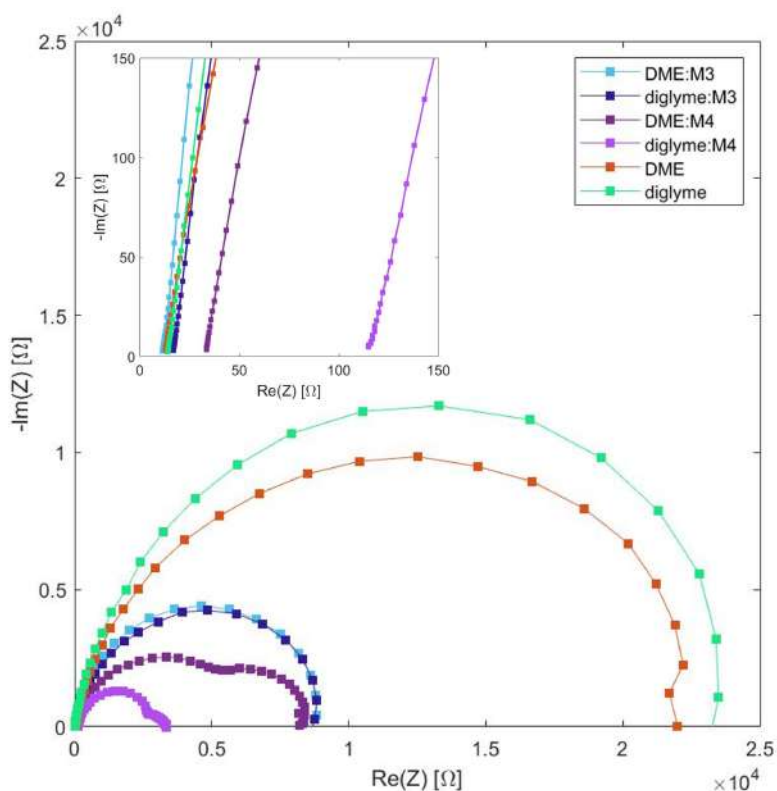


Figure 4.14: Nyquist plot showing the impedance of $\text{Mg}||\text{Mg}$ cells with different electrolytes containing 0.5 M $\text{Mg}(\text{TFSI})_2$ over a 20 kHz - 1 cHz frequency span. The squares represent measurement points of different frequencies. The solvent–additive configuration for each electrolyte is stated for each colour. All additive containing electrolytes have a 1:4 molar ratio between Mg ions and additive (original conc.). The figure shows a decrease in impedance for electrolytes containing the additive. The graph inserted in the upper left corner shows a close up of the high frequency region, which relates to the solution resistances of the electrolytes. Electrolytes containing M4 exhibit notably larger solution resistances compared to the other electrolytes.

Solution resistance measurements were repeated several times for the Mg||Mg cells and the trend of Figure 4.14 was maintained. The exact value did however scatter widely. This is a consequence of the reactivity of the Mg foil in combination with the separators, which can also interfere with the result. In order to obtain more reliable results, an EIS measurement was performed in a cell designed specifically for ion conduction measurements. Results are presented in Figure 4.15. The calculation of ionic conductivity (6.8, 6.3 and 3.4 mS/cm for E_{blank}, E3 and E4 respectively) is almost in agreement with values found in the literature (6.5, 5.3 and 4.0 mS/cm for E_{blank}, E3 and E4 respectively) [7]. Temperature differences during measurement pose a potential source of error.

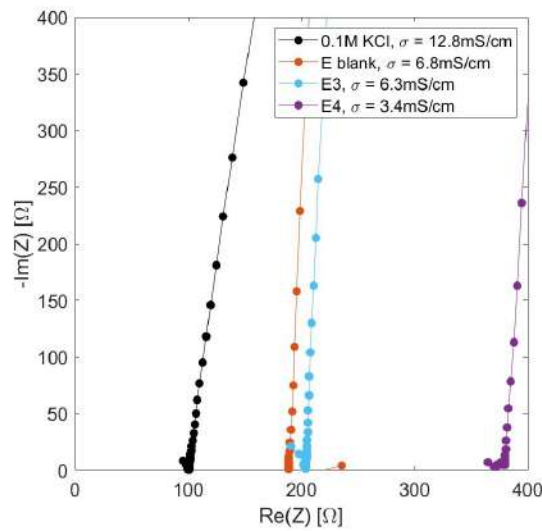


Figure 4.15: Nyquist plot from conductivity cell measurements. Performed on 1 MHz–1 Hz frequency span with SS||SS and Pt||Pt configurations of electrodes. 0.1 M KCl acts as a reference and the cell constant is calculated from its known ionic conductivity to deduce the parameter for the other electrolytes.

5

Conclusions and Outlook

The performance of RMBs can be significantly improved by employing methoxyethyl-amine chelants as an electrolyte additive. This was concluded through a combination of experimental methods — galvanostatic cycling, a composition and morphology study of deposits and through analysis of interfacial and electrolyte bulk impedance. The additives enhance ion transport and further promote redox reversibility and reduce cell losses. The main arguments for this statement are the high coulombic efficiency, low overpotential, high Mg purity of deposits and low interfacial impedance recorded for electrolytes containing the additive. The additives were also found to be compatible with the organic cathode material PAQS-CNT, displaying good capacity utilization. However, poor resilience towards higher current densities still remains a challenge and the problem of the low ionic conductivity imposed by the additive needs to be overcome as well. The project was inspired by Hou et al.'s presentation of methoxyethyl-amine chelants enabling Mg ion selective solvation shells and it should be noted that the performance promised in the article could not be replicated.

Electrolytes of 0.5 M $\text{Mg}(\text{TFSI})_2$:glyme were found to receive the largest performance boost from the additive in comparison to electrolytes containing MgCl_2 and $\text{Mg}(\text{Bhfp})_2$ salts and were therefore selected for further investigations. By varying the molar ratio between salt and additive an average coulombic efficiency of 96.9% spanning 100 cycles was reached (the corresponding value for electrolyte without additive is 44.3%). The optimal molar ratio was found to be close to 1:6. Surprisingly, the electrolyte with this additive concentration separates into two immiscible phases. The phenomenon poses an intriguing topic for further investigation — is the origin related to temperature and what is the electrolytes state and phase distribution during cycling? A second lingering curiosity is how larger electrode surface areas would impact performance with additive-containing electrolytes and how an electrolyte should be designed to maintain stability for such experiments.

Deposited species formed in the presence of the additive are generally larger and exhibit higher Mg purity, which indicates that the additive suppresses side reactions and imposes good ion transport at the electrode surface. The very same conclusion was also drawn from EIS analysis, where interfacial impedance was found to be remarkably low for electrolytes containing the additive. Similar studies extending to cathodes could enable further understanding of how the additive influences ion transport.

Bibliography

- [1] Michel Armand and J-M Tarascon. Building better batteries. *Nature*, 451(7179):652–657, 2008.
- [2] Benjamin K Sovacool. The precarious political economy of cobalt: Balancing prosperity, poverty, and brutality in artisanal and industrial mining in the Democratic Republic of the Congo. *The Extractive Industries and Society*, 6(3):915–939, 2019.
- [3] Alexandre Ponrouch, Jan Bitenc, Robert Dominko, Niklas Lindahl, Patrik Johansson, and M Rosa Palacín. Multivalent rechargeable batteries. *Energy Storage Materials*, 20:253–262, 2019.
- [4] Yaosen Tian, Guobo Zeng, Ann Rutt, Tan Shi, Haegyeom Kim, Jingyang Wang, Julius Koettgen, Yingzhi Sun, Bin Ouyang, Tina Chen, et al. Promises and challenges of next-generation “Beyond Li-ion” batteries for electric vehicles and grid decarbonization. *Chemical reviews*, 121(3):1623–1669, 2020.
- [5] Markus Jäckle, Katharina Helmbrecht, Malte Smits, Daniel Stottmeister, and Axel Groß. Self-diffusion barriers: possible descriptors for dendrite growth in batteries? *Energy & Environmental Science*, 11(12):3400–3407, 2018.
- [6] Ran Attias, Michael Salama, Baruch Hirsch, Yosef Goffer, and Doron Aurbach. Anode-electrolyte interfaces in secondary magnesium batteries. *Joule*, 3(1):27–52, 2019.
- [7] Singyuk Hou, Xiao Ji, Karen Gaskell, Peng-fei Wang, Luning Wang, Jijian Xu, Ruimin Sun, Oleg Borodin, and Chunsheng Wang. Solvation sheath reorganization enables divalent metal batteries with fast interfacial charge transfer kinetics. *Science*, 374(6564):172–178, 2021.
- [8] Alessandro Volta. XVII. On the electricity excited by the mere contact of conducting substances of different kinds. In a letter from Mr. Alexander Volta, FRS Professor of Natural Philosophy in the University of Pavia, to the Rt. Hon. Sir Joseph Banks, Bart. KBPR S. *Philosophical transactions of the Royal Society of London*, (90):403–431, 1800.
- [9] Kang Xu. Nonaqueous liquid electrolytes for lithium-based rechargeable batteries. *Chemical reviews*, 104(10):4303–4418, 2004.
- [10] Cornelia Breitkopf and Karen Swider-Lyons. *Springer handbook of electrochemical energy*. Springer, 2017.
- [11] Nav Nidhi Rajput, Xiaohui Qu, Niya Sa, Anthony K Burrell, and Kristin A Persson. The coupling between stability and ion pair formation in magnesium electrolytes from first-principles quantum mechanics and classical molecular dynamics. *Journal of the American Chemical Society*, 137(9):3411–3420, 2015.

-
- [12] Allen J Bard and Larry R Faulkner. *Electrochemical Methods, Fundamentals and Applications*. John Wiley sons, inc., 2nd edition, 2001.
- [13] Rabeb Grissa, Vincent Fernandez, Neal Fairley, Jonathan Hamon, Nicolas Stephant, Julien Rolland, Renaud Bouchet, Margaud Lecuyer, Marc Deschamps, Dominique Guyomard, et al. XPS and SEM-EDX study of electrolyte nature effect on Li electrode in lithium metal batteries. *ACS Applied Energy Materials*, 1(10):5694–5702, 2018.
- [14] Miran Gaberšček. Understanding Li-based battery materials via electrochemical impedance spectroscopy. *Nature Communications*, 12(6513):1–4, 2021.
- [15] LW Gaddum and HE French. The electrolysis of Grignard solutions. *Journal of the American Chemical Society*, 49(5):1295–1299, 1927.
- [16] Thomas D Gregory, Ronald J Hoffman, and Richard C Winterton. Nonaqueous electrochemistry of magnesium: applications to energy storage. *Journal of the Electrochemical Society*, 137(3):775–780, 1990.
- [17] Doron Aurbach, Z Lu, Alex Schechter, Yossef Gofer, H Gizbar, R Turgeman, Y Cohen, Mordechai Moshkovich, and El Levi. Prototype systems for rechargeable magnesium batteries. *Nature*, 407(6805):724–727, 2000.
- [18] Jan Bitenc and Robert Dominko. Opportunities and challenges in the development of cathode materials for rechargeable Mg batteries. *Frontiers in Chemistry*, 6:634, 2018.
- [19] Jan Bitenc, Klemen Pirnat, Tanja Bančič, Miran Gaberšček, Boštjan Genorio, Anna Randon-Vitanova, and Robert Dominko. Anthraquinone-based polymer as cathode in rechargeable magnesium batteries. *ChemSusChem*, 8(24):4128–4132, 2015.
- [20] Ivgeni Shterenberg, Michael Salama, Hyun Deog Yoo, Yosef Gofer, Jin-Bum Park, Yang-Kook Sun, and Doron Aurbach. Evaluation of (CF₃SO₂)₂N-(TFSI) based electrolyte solutions for Mg batteries. *Journal of The Electrochemical Society*, 162(13):118–128, 2015.
- [21] John Muldoon, Claudiu B Bucur, Allen G Oliver, Jaroslav Zajicek, Gary D Allred, and William C Boggess. Corrosion of magnesium electrolytes: chlorides—the culprit. *Energy & Environmental Science*, 6(2):482–487, 2013.
- [22] Hui Dong, Yanliang Liang, Oscar Tutusaus, Rana Mohtadi, Ye Zhang, Fang Hao, and Yan Yao. Directing Mg-storage chemistry in organic polymers toward high-energy Mg batteries. *Joule*, 3(3):782–793, 2019.
- [23] Zhirong Zhao-Karger, Maria Elisa Gil Bardaji, Olaf Fuhr, and Maximilian Fichtner. A new class of non-corrosive, highly efficient electrolytes for rechargeable magnesium batteries. *Journal of Materials Chemistry A*, 5(22):10815–10820, 2017.
- [24] William E Geiger and Frédéric Barrière. Organometallic electrochemistry based on electrolytes containing weakly-coordinating fluoroarylborate anions. *Accounts of chemical research*, 43(7):1030–1039, 2010.
- [25] Michael Salama, Ivgeni Shterenberg, Haim Gizbar, Neta N Eliaz, Monica Kosa, Keren Keinan-Adamsky, Michal Afri, Linda JW Shimon, Hugo E Gottlieb, Dan T Major, et al. Unique behavior of dimethoxyethane (DME)/Mg(N(SO₂CF₃)₂)₂ solutions. *The Journal of Physical Chemistry C*, 120(35):19586–19594, 2016.

- [26] Claudiu B Bucur, Thomas Gregory, Allen G Oliver, and John Muldoon. Confession of a magnesium battery. *The journal of physical chemistry letters*, 6(18):3578–3591, 2015.
- [27] Markus S Ding, Thomas Diemant, R Jürgen Behm, Stefano Passerini, and Guinevere A Giffin. Dendrite growth in mg metal cells containing Mg (TFSI)₂/glyme electrolytes. *Journal of The Electrochemical Society*, 165(10):1983–1990, 2018.
- [28] Zhirong Zhao-Karger, Runyu Liu, Wenxu Dai, Zhenyou Li, Thomas Diemant, BP Vinayan, Christian Bonatto Minella, Xingwen Yu, Arumugam Manthiram, R Jürgen Behm, et al. Toward highly reversible magnesium–sulfur batteries with efficient and practical Mg [B (hfp)₄]₂ electrolyte. *ACS Energy Letters*, 3(8):2005–2013, 2018.
- [29] Zhiping Song, Hui Zhan, and Yunhong Zhou. Anthraquinone based polymer as high performance cathode material for rechargeable lithium batteries. *Chemical communications*, (4):448–450, 2009.

DEPARTMENT OF PHYSICS
CHALMERS UNIVERSITY OF TECHNOLOGY
Gothenburg, Sweden
www.chalmers.se



CHALMERS
UNIVERSITY OF TECHNOLOGY